



Spin pumping and inverse spin Hall voltages from dynamical antiferromagnets

Øyvind Johansen* and Arne Brataas

Department of Physics, Norwegian University of Science and Technology, NO-7491 Trondheim, Norway

(Received 13 February 2017; published 20 June 2017)

Dynamical antiferromagnets can pump spins into adjacent conductors. The high antiferromagnetic resonance frequencies represent a challenge for experimental detection, but magnetic fields can reduce these resonance frequencies. We compute the ac and dc inverse spin Hall voltages resulting from dynamical spin excitations as a function of a magnetic field along the easy axis and the polarization of the driving ac magnetic field perpendicular to the easy axis. We consider the insulating antiferromagnets MnF_2 , FeF_2 , and NiO . Near the spin-flop transition, there is a significant enhancement of the dc spin pumping and inverse spin Hall voltage for the uniaxial antiferromagnets MnF_2 and FeF_2 . In the uniaxial antiferromagnets it is also found that the ac spin pumping is independent of the external magnetic field when the driving field has the optimal circular polarization. In the biaxial NiO , the voltages are much weaker, and there is no spin-flop enhancement of the dc component.

DOI: [10.1103/PhysRevB.95.220408](https://doi.org/10.1103/PhysRevB.95.220408)

Spin pumping is a versatile tool for probing spin dynamics in ferromagnets [1–6]. The magnitude of the pumped spin currents reveals information about the magnetization dynamics and the electron-magnon coupling at interfaces [7–9]. The precessing spins generate a pure spin flow into adjacent conductors. Inside the conductor, the resulting spin accumulation and currents give insight into the spin-orbit coupling. The inverse spin Hall effect (ISHE) is often used to convert the pure spin current into a charge current, which is detected [10,11]. Additionally, the induced nonequilibrium spins can be probed with x-ray magnetic circular dichroism measurements [12,13].

Antiferromagnets differ strikingly from ferromagnets [14]. There are no stray fields in antiferromagnets, making them more robust against the influence of external magnetic fields. The recent discovery of anisotropic magnetoresistance [15–17], spin-orbit torques [18], and electrical switching of an antiferromagnet [19] demonstrate the feasibility of antiferromagnets as active spintronics components.

The real benefit of antiferromagnets is that they can enable terahertz circuits. Unlike ferromagnets, the resonance frequency of antiferromagnets is also governed by the tremendous exchange energy. We recently demonstrated that the transverse spin conductance, a governing factor of spin pumping, is as large in antiferromagnet–normal metal junctions (AF/N) as in ferromagnet–normal metal junctions [20]. Furthermore, this result is valid even when the magnetic system is insulating. The firm electron-magnon coupling at the interface opens the door for electrical probing of the ultrafast spin dynamics in antiferromagnets [20,21].

Precessing spins in antiferromagnets generate terahertz currents in adjacent conductors. This ability opens new territory in high-frequency spintronics. Such studies could become influential in gathering vital insight into fast electron dynamics and eventually for a broad range of applications. These electric signals also provide further knowledge about the less explored field of antiferromagnetic spin dynamics. This potential requires thorough exploration; we need to establish several critical aspects.

The manner in which spin pumping generates ac and dc inverse spin Hall voltages has yet to be studied in detail.

Furthermore, there is a large variety of antiferromagnets and external field configurations that require knowledge beyond the first predictions of the magnitude of the pumped spin current of Ref. [20]. Recently, researchers explored spin transport through, e.g., the insulating antiferromagnets NiO and MnF_2 . Unlike the treatment of Ref. [20], in NiO , there are two significant anisotropies to consider. As a starting point in the exploration of high-frequency spintronics, it is also important to tune the resonance frequencies to a lower gigahertz range for easier detection by conventional electronics. The application of an external magnetic field can lower the resonance frequency. However, the details of the magnetic field and its ac component polarization dependence also remain to be classified, a task that we will perform here.

In this Rapid Communication, we compute the inverse spin Hall ac and dc voltages generated by spin pumping. We hope that our studies will further motivate these voltages to be experimentally measured. Such studies will provide a needed deeper insight into antiferromagnetic resonance phenomena, features much less explored than their ferromagnetic counterparts in recent decades.

We consider an insulating antiferromagnet–normal metal bilayer, as illustrated in Fig. 1. We also consider a variety of magnetic anisotropies and magnetic field configurations and strengths. Therefore, the results apply to more complex systems such as biaxial antiferromagnets with elliptical precessional modes. The model also accounts for spin backflow due to the spin accumulation in the metal. We also study how the inverse spin Hall voltages depend on the polarization of the ac magnetic field for different systems, which we find to have a strong influence on the resulting signal. Our main findings are that, when applying an external magnetic field along the easy axis close to the spin-flop transition, we can decrease the resonance frequency while simultaneously significantly increasing the inverse spin Hall signal. The increase in the signal can even overcome the previously anticipated limiting factor in antiferromagnet spin pumping: the ratio of the anisotropic energy to the exchange energy [20].

We consider a small antiferromagnet in the macrospin limit whereby all spin excitations are homogeneous. The antiferromagnet has two sublattices, with temporal magnetizations \mathbf{M}_1 and \mathbf{M}_2 . The dynamics are described by the

*Corresponding author: oyvinjoh@ntnu.no

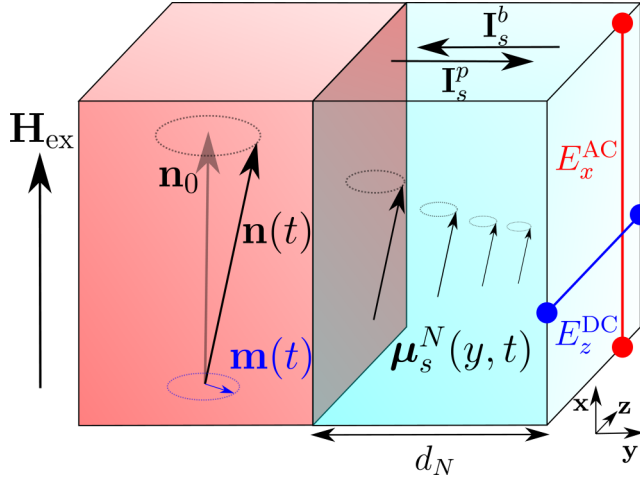


FIG. 1. The precession of \mathbf{m} and \mathbf{n} around their equilibrium values pumps spins into the adjacent normal metal of thickness d_N . In turn, the spin accumulation μ_s^N in the normal metal causes a backflow of spins into the antiferromagnet. The spin current in the normal metal causes ac and dc electric fields in the x and z directions, respectively, through the inverse spin Hall effect.

staggered magnetizations $\mathbf{L} = (\mathbf{M}_1 - \mathbf{M}_2)/2 = L\mathbf{n}$ and the magnetization $\mathbf{M} = (\mathbf{M}_1 + \mathbf{M}_2)/2 = L\mathbf{m}$. These fields satisfy the constraints $\mathbf{n}^2 + \mathbf{m}^2 = 1$ and $\mathbf{n} \cdot \mathbf{m} = 0$. At equilibrium, the sublattice magnetizations are antiparallel. An ac magnetic field, with a general polarization, drives the magnetic moments at resonance.

The antiferromagnets that we consider are described by the free energy

$$F = \frac{LV}{\gamma} [\omega_E(\mathbf{m}^2 - \mathbf{n}^2) + \omega_\perp(m_z^2 + n_z^2) - \omega_\parallel(m_x^2 + n_x^2) - 2\omega_x m_x - 2\omega_y m_y - 2\omega_z m_z], \quad (1)$$

where γ is the gyromagnetic ratio, V is the volume of the antiferromagnet, $\omega_E \geq 0$ is the exchange frequency, and $\omega_\perp \geq 0$ and $\omega_\parallel \geq 0$ are the hard axis (z axis) and easy axis (x axis) anisotropy frequencies. The frequency ω_x quantifies the influence of the external magnetic field along the easy axis, whereas ω_y and ω_z quantify the influence of the ac magnetic field in the yz plane. In Table I, we list the exchange and anisotropy frequencies for MnF_2 , FeF_2 , and NiO .

The dynamic Landau-Lifshitz-Gilbert (LLG) equations that describe the precession of \mathbf{n} and \mathbf{m} are

$$\dot{\mathbf{n}} = \frac{1}{2}(\omega_m \times \mathbf{n} + \omega_n \times \mathbf{m}) + \boldsymbol{\tau}_n, \quad (2a)$$

$$\dot{\mathbf{m}} = \frac{1}{2}(\omega_n \times \mathbf{n} + \omega_m \times \mathbf{m}) + \boldsymbol{\tau}_m, \quad (2b)$$

TABLE I. Exchange and anisotropy frequencies.

Material	ω_E (10^{12} s^{-1})	ω_\parallel (10^{12} s^{-1})	ω_\perp (10^{12} s^{-1})
MnF_2 [22]	9.3	1.5×10^{-1}	
FeF_2 [23]	9.5	3.5	
NiO [24,25]	1.7×10^2	2.3×10^{-3}	1.3×10^{-1}

with the effective fields $\omega_n = -(\gamma/L)\partial F/\partial \mathbf{n}$ and $\omega_m = -(\gamma/L)\partial F/\partial \mathbf{m}$. The dissipation and spin-pumping torques are

$$\boldsymbol{\tau}_n = \alpha[\mathbf{n} \times \dot{\mathbf{m}} + \mathbf{m} \times \dot{\mathbf{n}}], \quad (3a)$$

$$\boldsymbol{\tau}_m = \alpha[\mathbf{n} \times \dot{\mathbf{n}} + \mathbf{m} \times \dot{\mathbf{m}}], \quad (3b)$$

where the total Gilbert damping coefficient α is a sum of the intrinsic damping and the spin-pumping-enhanced damping: $\alpha = \alpha_0 + \alpha_{\text{SP}}$ [20,26].

A linear response expansion around the equilibrium values of \mathbf{n} and \mathbf{m} determines the antiferromagnetic resonance (AFMR) frequencies. For simplicity, we only present the resonance frequencies in the exchange limit $\omega_\parallel, \omega_\perp \ll \omega_E$. This limit is valid for many antiferromagnets but not for FeF_2 due to a large anisotropy. In our numerical calculations below, we do not make this approximation. In the exchange limit, the four resonance frequencies below spin flop are [27]

$$\omega_{\text{res}}^2 \approx \omega_x^2 + \omega_0^2 \pm \sqrt{\omega_E^2 \omega_\perp^2 + 4\omega_x^2 \omega_0^2}, \quad (4)$$

where $\omega_0^2 = \omega_E(2\omega_\parallel + \omega_\perp)$. The critical field strength at which the spin-flop transition occurs is $|\omega_x^{\text{crit}}| = \sqrt{\omega_\parallel(2\omega_E + \omega_\perp)}$ in both uniaxial and biaxial antiferromagnets. We will only consider magnetic fields below this value.

Herein, we focus on the right-handed low-energy mode since we want to decrease the resonance frequency. In the absence of an external magnetic field, the resonance frequency of this mode is 0.27 THz for MnF_2 , 1.41 THz for FeF_2 , and 0.14 THz for NiO . By applying a magnetic field close to the spin-flop transition, we can reduce these resonance frequencies down to the gigahertz range. Such a reduction should enable detection of AFMR and the resulting significant spin-pumping-induced ac and dc ISHE voltages.

The pumped spin current from a dynamical antiferromagnet into a normal metal is [20]

$$\mathbf{I}_s^p = \frac{\hbar g_\perp}{2\pi} (\mathbf{n} \times \dot{\mathbf{n}} + \mathbf{m} \times \dot{\mathbf{m}}), \quad (5)$$

where g_\perp is the transverse (“mixing”) conductance. The spin pumping from the antiferromagnetic insulator causes a spin accumulation in the normal metal, which in turn produces a spin backflow current [11]. In antiferromagnetic insulators, the backflow spin currents within the sublattices add constructively [20,28]:

$$\mathbf{I}_s^b = -\frac{g_\perp}{2\pi} [\mathbf{m} \times (\boldsymbol{\mu}_s^N \times \mathbf{m}) + \mathbf{n} \times (\boldsymbol{\mu}_s^N \times \mathbf{n})], \quad (6)$$

where $\boldsymbol{\mu}_s^N$ is the spin accumulation in the normal metal.

The most significant contributions to the spin current are second order in the deviations from equilibrium along the easy axis and first order along the perpendicular directions. Nevertheless, the leading-order terms in the total spin current only depend on the first-order deviations of the magnetic moments from their equilibrium values, $\mathbf{n}_0 = \mathbf{e}_x$ and $\mathbf{m}_0 = \mathbf{0}$. It is therefore sufficient to consider the linear response expansions

$$\mathbf{n} = \mathbf{n}_0 + \frac{1}{2}(\delta \mathbf{n} e^{i\omega t} + \delta \mathbf{n}^* e^{-i\omega t}), \quad (7a)$$

$$\mathbf{m} = \frac{1}{2}(\delta \mathbf{m} e^{i\omega t} + \delta \mathbf{m}^* e^{-i\omega t}), \quad (7b)$$

where the transverse deviations are $\delta\mathbf{n} = \delta n_y \mathbf{e}_y + \delta n_z \mathbf{e}_z$ and $\delta\mathbf{m} = \delta m_y \mathbf{e}_y + \delta m_z \mathbf{e}_z$. ω is the driving frequency of the ac magnetic field.

The spin accumulation μ_s^N is a solution of the spin diffusion equation

$$\frac{\partial \mu_s^N(\mathbf{r}, t)}{\partial t} = \gamma_N \mathbf{H}_{\text{ex}} \times \mu_s^N + D_N \frac{\partial^2 \mu_s^N}{\partial y^2} - \frac{\mu_s^N}{\tau_{\text{sf}}^N}, \quad (8)$$

where the terms on the right-hand side of Eq. (8) are properties of the normal metal such as the diffusion coefficient D_N , the gyromagnetic ratio γ_N , and the spin-flip relaxation time τ_{sf}^N , and \mathbf{H}_{ex} is the external magnetic field. The boundary conditions for μ_s^N require that the spin current vanishes at the outer edge of the normal metal ($y = d_N$) and that the current is continuous across the antiferromagnet–normal metal interface ($y = 0$). The diffusion equation can be solved in position-frequency space [11,29] in terms of the Fourier components of the total spin current $\mathbf{I}_s^N = \mathbf{I}_s^p + \mathbf{I}_s^b$ at $y = 0$.

The spin current in the normal metal causes a charge current perpendicular to the spin current's direction and polarization through the ISHE. This charge current is given by [30,31]

$$\mathbf{j}_c^{\text{ISHE}}(y, t) = \theta_N \frac{2e}{A\hbar} \mathbf{e}_y \times \mathbf{I}_s^N(y, t), \quad (9)$$

where θ_N is the spin Hall angle in the normal metal and A is the area of the AF|N interface. Since the system is an open circuit, the charge current accumulates charges at the interfaces. In turn, a generated electric field ensures that the net charge current through the metal vanishes. To determine this electric field, we integrate the charge current $\mathbf{j}_c^{\text{ISHE}}$ over the metallic system to find the electric field needed to cancel the charge current. See the Supplemental Material [32] for the full derivation. The dc component of this electric field becomes

$$E_z^{\text{dc}} = \varepsilon_N \left(1 - \frac{1}{\cosh(d_N/\lambda_{\text{sd}}^N)} \right) \mu_0^x, \quad (10)$$

the first harmonic ac component is

$$E_x^{\text{ac}}(t) = \varepsilon_N \text{Re} \left[\left(\frac{\mu_1^z + i\mu_1^y}{\cosh[\kappa_3(\omega)d_N]} + \frac{\mu_1^z - i\mu_1^y}{\cosh[\kappa_2(\omega)d_N]} - 2\mu_1^z \right) e^{i\omega t} \right], \quad (11)$$

and the second harmonic ac component is

$$E_z^{\text{ac}}(t) = 2\varepsilon_N \text{Re} \left[\left(1 - \frac{1}{\cosh[\kappa_1(2\omega)d_N]} \right) \mu_2^x e^{2i\omega t} \right]. \quad (12)$$

Here, we have introduced the conversion coefficient $\varepsilon_N = \theta_N e \nu D_N / (\sigma_N d_N)$, where σ_N is the conductivity of the normal metal. The factors $\mu_n^{x/y/z}$ are the n th Fourier components of the spin accumulation at the AF|N interface ($y = 0$). We compute

that they are

$$\mu_1^y = -\frac{i\hbar\omega g_{\perp}}{4\pi} \frac{[\Gamma_2(\omega) + \frac{g_{\perp}}{2\pi}] \delta n_z + \Gamma_3(\omega) \delta n_y}{[\Gamma_2(\omega) + \frac{g_{\perp}}{2\pi}]^2 + \Gamma_3^2(\omega)}, \quad (13a)$$

$$\mu_1^z = \frac{i\hbar\omega g_{\perp}}{4\pi} \frac{[\Gamma_2(\omega) + \frac{g_{\perp}}{2\pi}] \delta n_y - \Gamma_3(\omega) \delta n_z}{[\Gamma_2(\omega) + \frac{g_{\perp}}{2\pi}]^2 + \Gamma_3^2(\omega)}, \quad (13b)$$

$$\mu_2^x = \frac{g_{\perp}}{4\pi\Gamma_1(2\omega)} (\mu_1^y \delta n_y + \mu_1^z \delta n_z) \quad (13c)$$

for the first and second harmonic ac components, and

$$\mu_0^x = \frac{g_{\perp}}{2\pi\Gamma_1(0)} [\text{Re}(\mu_1^y \delta n_y^* + \mu_1^z \delta n_z^*) - \hbar\omega \text{Im}(\delta n_y^* \delta n_z + \delta m_y^* \delta m_z)] \quad (14)$$

for the dc component. All other components of the spin accumulation vanish. The components of the spin accumulation of Eqs. (13) and (14) are expressed in terms of the functions

$$\Gamma_1(\omega) = \frac{1}{2} \hbar \nu A D_N \Lambda_1(\omega), \quad (15a)$$

$$\Gamma_2(\omega) = \frac{1}{4} \hbar \nu A D_N [\Lambda_2(\omega) + \Lambda_3(\omega)], \quad (15b)$$

$$\Gamma_3(\omega) = \frac{i}{4} \hbar \nu A D_N [\Lambda_2(\omega) - \Lambda_3(\omega)], \quad (15c)$$

with $\Lambda_i(\omega) = \kappa_i(\omega) \tanh[\kappa_i(\omega)d_N]$. Here, we have defined $\kappa_1^2 = (1 + i\omega\tau_{\text{sf}}^N)/(\lambda_{\text{sd}}^N)^2$, $\kappa_{2,3}^2 = \kappa_1^2 \mp i\gamma_N H_{\text{ex}}/D_N$, the spin diffusion length $\lambda_{\text{sd}}^N = \sqrt{D_N \tau_{\text{sf}}^N}$, and the one-spin density of state ν . Note that μ_2^x and consequently E_z^{ac} vanish in the absence of a magnetic field [$\Gamma_3(\omega) = 0$] and when the precession of the staggered magnetization is circular ($\delta n_z = \pm i \delta n_y$).

We will now use our model to compute the ISHE signal as a function of external magnetic fields in an AF|Pt bilayer. By inserting the linear response ansatz of Eq. (7) into the LLG equations in Eq. (2), we determine the functions $\delta\mathbf{n}$ and $\delta\mathbf{m}$. The components of the ac magnetic field that drives these perturbations are given by $\omega_j = |\omega_j| \exp(i\omega t + i\theta_j)$ for $j = y, z$. The phase difference $\theta_z - \theta_y$ determines the polarization of the ac field, and significantly affects the resulting spin current. In our calculations, we let $|\omega_y| = |\omega_z|$.

As the material properties of Pt, we use $\tau_{\text{sf}}^N = 0.01$ ps [11], $\nu = 4.55 \times 10^{47} \text{ J}^{-1} \text{ m}^{-3}$ [33], $\sigma_N = 5 \times 10^6 \text{ } (\Omega \text{ m})^{-1}$ [34], $\lambda_{\text{sd}}^N = 1.5$ nm, and $\theta_N = 0.075$ [35]. These properties are at 10 K. The transverse spin conductance g_{\perp} is of the same order of magnitude as that of a ferromagnetic or ferrimagnetic material [20]. We therefore estimate this to be $g_{\perp}/A = 3 \times 10^{18} \text{ m}^{-2}$ [36,37]. Experimental measurements of g_{\perp} are needed and are further motivated by the present calculations.

The magnitude of the ISHE signal depends on the thickness of the Pt layer. It increases approximately linearly with d_N for $d_N/\lambda_{\text{sd}}^N \ll 1$ and is inversely proportional to d_N for $d_N/\lambda_{\text{sd}}^N \gg 1$. This qualitative behavior is similar to that in ferromagnetic/normal metal bilayers (cf. Fig. 3(a) in Ref. [11]). The peak of the ISHE signal is at some value $d_N \sim \lambda_{\text{sd}}^N$, and for our choice of parameters, it peaks at $d_N \approx 0.8\lambda_{\text{sd}}^N = 1.2$ nm.

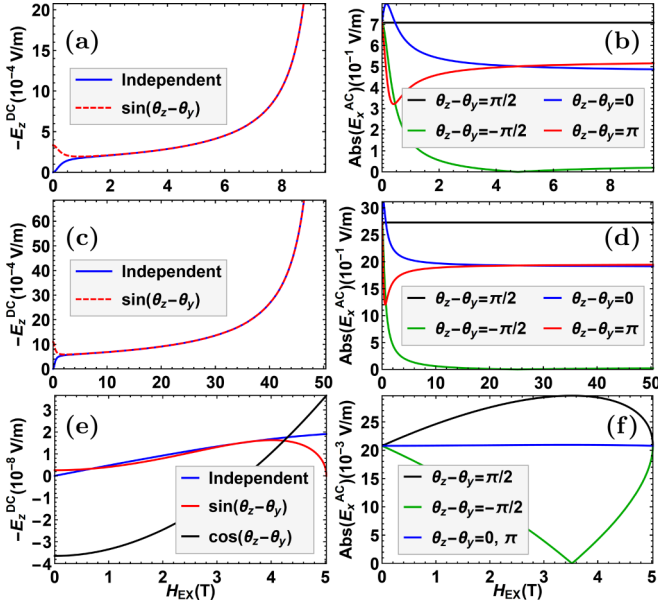


FIG. 2. dc and first harmonic ac components of the ISHE electric field for MnF_2 [(a) and (b)], FeF_2 [(c) and (d)], and NiO [(e) and (f)] as a function of external magnetic field along the easy axis for different polarizations of the ac magnetic field. The ac field is 1 mT, and $\alpha = 0.01$.

We use this thickness of the Pt layer for the remaining calculations. The optimal thickness d_N weakly depends on the value of g_{\perp}/A and should therefore be determined experimentally.

Figure 2 plots the dc and the first harmonic ac components of the ISHE electric field as a function of the magnetic field. In the uniaxial antiferromagnets, MnF_2 and FeF_2 , one contribution to the dc signal is independent of the ac magnetic field polarization, and the other contribution is proportional to $\sin(\theta_z - \theta_y)$. At high magnetic fields, these contributions are equal in magnitude but add constructively or destructively, depending on the circular polarization of the ac magnetic field.

Reference [20] demonstrated that the pumped dc spin current in uniaxial antiferromagnets at resonance is suppressed by the factor $\sqrt{\omega_{\parallel}/\omega_E}$. Since $\sqrt{\omega_{\parallel}/\omega_E}$ is significantly larger in FeF_2 (0.61) than in MnF_2 (0.13), it was believed that FeF_2 gives a stronger signal than does MnF_2 . However, with our present additional insight, we reach the opposite conclusion at finite magnetic fields. We find that when $\omega_x \rightarrow \omega_x^{\text{crit}}$, the dc signal diverges as $(\omega_x^{\text{crit}} - \omega_x)^{-1}$. The utilization of the divergence is a better route toward enhancing the ISHE signal than increasing $\sqrt{\omega_{\parallel}/\omega_E}$. This implies that MnF_2 is a more promising candidate than FeF_2 because the spin-flop field of MnF_2 (9.5 T) is easier to achieve experimentally than is that of FeF_2 (50.4 T).

The dc signal diverges because the linear response model breaks down close to the spin-flop transition. By analyzing the magnitude of $|\delta \mathbf{n}|$ we find that it is 0.01 at $\omega_x \approx 0.95\omega_x^{\text{crit}}$ and 0.1 at $\omega_x \approx 0.995\omega_x^{\text{crit}}$ for the uniaxial antiferromagnets. Consequently, linear response is a good approximation fairly close to the divergence. The enhancement of the dc spin pumping close to the spin-flop transition is therefore a real

phenomenon. We find that the breakdown of the linear response theory is even softer for the biaxial NiO .

Unlike the dc component, the first harmonic ac component is independent of the ac magnetic field polarization in the absence of a uniform external magnetic field and converges toward a finite value as $\omega_x \rightarrow \omega_x^{\text{crit}}$. The signal when the polarization is circular ($\theta_z - \theta_y = \pi/2$) gives the largest dc signal (and ac signal for sufficiently large magnetic fields). Furthermore, this curve becomes independent of the magnetic field. The origin of this is a complicated compensation between the diverging contributions from the out-of-equilibrium fields and the vanishing resonance frequency around the spin-flop transition.

In NiO , the dominant ac magnetic field contribution is linear in the polarization, which is proportional to $\cos(\theta_z - \theta_y)$. Such a feature appears when there is a hard axis, and the precession is in the easy plane. The linear contribution dominates when $\omega_{\perp}/\sqrt{\omega_E\omega_{\parallel}} \gg \alpha$. In biaxial antiferromagnets, we find that the pumped current is governed by the scaling factor $\alpha\omega_{\parallel}/\omega_{\perp}$ instead of $\sqrt{\omega_{\parallel}/\omega_E}$. In discussing the strength of the spin-pumping signals, we should also note that, in both uniaxial and easy-plane antiferromagnets, the signal is inversely proportional to ω_E . Since $\omega_{\parallel}/\omega_{\perp} \sim 0.02$ and since ω_E is exceptionally large in NiO , the dc spin pumping signal is weak in comparison to that of MnF_2 and FeF_2 . In addition, the dc signal in NiO does not exhibit a divergence as $\omega_x \rightarrow \omega_x^{\text{crit}}$. We do not present the second harmonic ac voltage since it is minimal (and in many cases identically zero). Our results imply that uniaxial antiferromagnets are preferred candidates for the observation of spin pumping compared to hard-axis antiferromagnets such as NiO .

Reference [22] conducted preliminary spin-pumping experiments for a $\text{MnF}_2|\text{Pt}$ system. However, they attributed the dominant dc signal to microwave rectification and not spin pumping. Nevertheless, they observed a small change in the signal upon reversal of the magnetic field, which is consistent with spin pumping.

We propose a different experimental geometry to enhance the spin-pumping signal. The use of the ac magnetic field in a plane perpendicular to the easy axis and a polarization $\theta_z - \theta_y = \pi/2$ increases the dc ISHE signal by a factor of 4. Additionally, by reducing the thickness of the Pt layer from 7 nm to the thickness where the ISHE signal attains its maximum (in our calculations, this is 1.2 nm), we can further amplify the signal by a factor of 2. Together, these improvements will increase the signal strength by an order of magnitude. Whether the signal is due to spin pumping can then easily be tested by the dependence on the polarization of the ac magnetic field according to our model. A circular polarization with $\theta_z - \theta_y = \pi/2$ doubles the signal strength compared to a linear polarization. On the other hand, a circular polarization with $\theta_z - \theta_y = -\pi/2$ results in no dc spin pumping. In contrast, microwave rectification effects should be much less sensitive to the polarization.

In summary, we computed the inverse spin Hall signal as a result of spin pumping and spin backflow in an AF|N bilayer. Our results apply to any polarization of the ac magnetic field and precessional motion of the magnetizations, and the results can also be used in more complex biaxial antiferromagnets. We demonstrate that the dc signal increases substantially near the

spin-flop transition in uniaxial antiferromagnets. Furthermore, the signal strongly depends on the polarization of the ac magnetic field. We also suggest an improved experimental geometry that considerably enhances the dc signal resulting from spin pumping.

The research leading to these results has received funding from the European Research Council via Advanced Grant No. 669442 “Insulatronics”, EU FET “Transpire” via Grant No. 737038, and The Research Council of Norway via Grant No. 239926.

-
- [1] S. Mizukami, Y. Ando, and T. Mizusaki, *Jpn. J. Appl. Phys.* **40**, 580 (2001).
- [2] R. Urban, G. Woltersdorf, and B. Heinrich, *Phys. Rev. Lett.* **87**, 217204 (2001).
- [3] Y. Tserkovnyak, A. Brataas, and G. E. W. Bauer, *Phys. Rev. Lett.* **88**, 117601 (2002).
- [4] A. Brataas, Y. Tserkovnyak, G. E. W. Bauer, and B. I. Halperin, *Phys. Rev. B* **66**, 060404 (2002).
- [5] B. Heinrich, Y. Tserkovnyak, G. Woltersdorf, A. Brataas, R. Urban, and G. E. W. Bauer, *Phys. Rev. Lett.* **90**, 187601 (2003).
- [6] Y. Tserkovnyak, A. Brataas, G. E. W. Bauer, and B. I. Halperin, *Rev. Mod. Phys.* **77**, 1375 (2005).
- [7] M. V. Costache, M. Sladkov, S. M. Watts, C. H. van der Wal, and B. J. van Wees, *Phys. Rev. Lett.* **97**, 216603 (2006).
- [8] B. Heinrich, C. Burrowes, E. Montoya, B. Kardasz, E. Girt, Y.-Y. Song, Y. Sun, and M. Wu, *Phys. Rev. Lett.* **107**, 066604 (2011).
- [9] A. Kapelrud and A. Brataas, *Phys. Rev. Lett.* **111**, 097602 (2013).
- [10] O. Mosendz, J. E. Pearson, F. Y. Fradin, G. E. W. Bauer, S. D. Bader, and A. Hoffmann, *Phys. Rev. Lett.* **104**, 046601 (2010).
- [11] H. J. Jiao and G. E. W. Bauer, *Phys. Rev. Lett.* **110**, 217602 (2013).
- [12] M. K. Marcham, L. R. Shelford, S. A. Cavill, P. S. Keatley, W. Yu, P. Shafer, A. Neudert, J. R. Childress, J. A. Katine, E. Arenholz, N. D. Telling, G. van der Laan, and R. J. Hicken, *Phys. Rev. B* **87**, 180403 (2013).
- [13] A. A. Baker, A. I. Figueroa, C. J. Love, S. A. Cavill, T. Hesjedal, and G. van der Laan, *Phys. Rev. Lett.* **116**, 047201 (2016).
- [14] T. Jungwirth, X. Marti, P. Wadley, and J. Wunderlich, *Nat. Nanotechnol.* **11**, 231 (2016).
- [15] B. G. Park, J. Wunderlich, X. Marti, V. Holý, Y. Kurosaki, M. Yamada, H. Yamamoto, A. Nishide, J. Hayakawa, H. Takahashi, A. B. Shick, and T. Jungwirth, *Nat. Mater.* **10**, 347 (2011).
- [16] X. Marti, B. G. Park, J. Wunderlich, H. Reichlová, Y. Kurosaki, M. Yamada, H. Yamamoto, A. Nishide, J. Hayakawa, H. Takahashi, and T. Jungwirth, *Phys. Rev. Lett.* **108**, 017201 (2012).
- [17] H. Wang, C. Du, P. C. Hammel, and F. Yang, *Phys. Rev. Lett.* **113**, 097202 (2014).
- [18] J. Železný, H. Gao, K. Výborný, J. Zemen, J. Mašek, A. Manchon, J. Wunderlich, J. Sinova, and T. Jungwirth, *Phys. Rev. Lett.* **113**, 157201 (2014).
- [19] P. Wadley, B. Howells, J. Železný, C. Andrews, V. Hills, R. P. Campion, V. Novák, K. Olejník, F. Maccherozzi, S. S. Dhesi, S. Y. Martin, T. Wagner, J. Wunderlich, F. Freimuth, Y. Mokrousov, J. Kuneš, J. S. Chauhan, M. J. Grzybowski, A. W. Rushforth, K. W. Edmonds, B. L. Gallagher, and T. Jungwirth, *Science* **351**, 587 (2016).
- [20] R. Cheng, J. Xiao, Q. Niu, and A. Brataas, *Phys. Rev. Lett.* **113**, 057601 (2014).
- [21] R. Cheng, D. Xiao, and A. Brataas, *Phys. Rev. Lett.* **116**, 207603 (2016).
- [22] M. P. Ross, Spin dynamics in an antiferromagnet, Ph.D. thesis, Technische Universität München, 2013.
- [23] R. C. Ohlmann and M. Tinkham, *Phys. Rev.* **123**, 425 (1961).
- [24] T. Satoh, S.-J. Cho, R. Iida, T. Shimura, K. Kuroda, H. Ueda, Y. Ueda, B. A. Ivanov, F. Nori, and M. Fiebig, *Phys. Rev. Lett.* **105**, 077402 (2010).
- [25] M. T. Hutchings and E. J. Samuelsen, *Phys. Rev. B* **6**, 3447 (1972).
- [26] K. M. D. Hals, Y. Tserkovnyak, and A. Brataas, *Phys. Rev. Lett.* **106**, 107206 (2011).
- [27] K. Yosida, *Prog. Theor. Phys.* **7**, 25 (1952).
- [28] H. V. Gomonay and V. M. Loktev, *Phys. Rev. B* **81**, 144427 (2010).
- [29] M. Johnson and R. H. Silsbee, *Phys. Rev. B* **37**, 5312 (1988).
- [30] E. Saitoh, M. Ueda, H. Miyajima, and G. Tatara, *Appl. Phys. Lett.* **88**, 182509 (2006).
- [31] O. Mosendz, V. Vlaminc, J. E. Pearson, F. Y. Fradin, G. E. W. Bauer, S. D. Bader, and A. Hoffmann, *Phys. Rev. B* **82**, 214403 (2010).
- [32] See Supplemental Material at <http://link.aps.org/supplemental/10.1103/PhysRevB.95.220408> for the detailed derivations.
- [33] D. Papaconstantopoulos, *Handbook of the Band Structure of Elemental Solids* (Plenum, New York, 1986).
- [34] L. Liu, R. A. Buhrman, and D. C. Ralph, [arXiv:1111.3702](https://arxiv.org/abs/1111.3702).
- [35] S. Meyer, M. Althammer, S. Geprägs, M. Opel, R. Gross, and S. T. B. Goennenwein, *Appl. Phys. Lett.* **104**, 242411 (2014).
- [36] T. Yoshino, K. Ando, K. Harii, H. Nakayama, Y. Kajiwara, and E. Saitoh, *J. Phys.: Conf. Ser.* **266**, 012115 (2011).
- [37] M. Haertinger, C. H. Back, J. Lotze, M. Weiler, S. Geprägs, H. Huebl, S. T. B. Goennenwein, and G. Woltersdorf, *Phys. Rev. B* **92**, 054437 (2015).